JOURNAL OF AIRCRAFT
Vol. 38, No. 5, September–October 2001

Evaluation of Scaling Approach for Stiffened Composite Flat Panels Loaded in Compression

Marshall Rouse*
NASA Langley Research Center, Hampton, Virginia 23681-2199
and
Mahyar Assadi†
Boeing Commercial Airplane Group, Renton, Washington 98055

Results of an experimental study of the effects of geometric scaling on a graphite-epoxy flat stiffened-skin panel concept loaded in compression are presented. The scaled models were fabricated using an approach to laminate thickness scaling, referred to as the "ply-thickness method." The structural response and failure characteristics of full-, half-, and quarter-scale specimens fabricated with this scaling concept are discussed and compared. The scaled-up failure loads of the half- and quarter-scale models agree well with the failure load of the full-scale prototypes tested. The strength scale effects observed in the results were substantially smaller than those in earlier studies that employed other laminate scaling techniques. The experimental results indicate that failure initiated by crippling and delamination in the cap of the longitudinal stiffeners and skin-stiffener separation at the bond lines was followed by failure of the specimen skin. Nonlinear finite element analysis results correlate well with experimental results up to failure.

Introduction

THE application of composite materials to aerospace structures has been shown to improve structural efficiency because of the high stiffness-to-weight and strength-to-weight ratios for these structures. To understand better the structural behavior of aerospace structures that are fabricated from composite materials, large structural subcomponents are usually designed and tested. Because large subcomponents are expensive to fabricate and test, structural scaling approaches have been investigated wherein smaller models are fabricated and tested to provide results that can be used to develop and design full-scale composite structures. Several researchers have investigated scale-up effects on the strength of coupon specimens fabricated from composite materials (e.g., Refs. 1 and 2). Scale-up effects on the buckling, postbuckling, and crippling of composite stiffeners have also been investigated.[3] An analytical study of the effects of scale-up on the structural response of built-up structures has also been reported.[4] However, the effects of scaling in complex composite structures have not been adequately investigated. Moreover, the traditional approaches to laminate thickness scaling have often proven unsatisfactory (e.g., Refs. 1 and 5) caused, in part, by their inability to model the interply bond mechanism.

The present paper presents the results of an experimental and analytical study into the buckling response and failure of full-, half- and quarter-scale flat stiffened-skin graphite-epoxy panels subjected to compressive uniaxial loads. The specimens tested in this investigation were designed to have the same buckling strain, regardless of their geometric scale. A key to achieving this form of similitude is the invariance of the response-critical constitutive properties between the full-scale prototype and the subscale models. The present study utilizes an approach to laminate thickness scaling, which is referred to herein as the "ply-thickness method." This approach utilizes scaled-thickness plies that possess the same resin content percentage (by weight) as the full-scale plies. The size and type of fibers in the scaled-thickness plies remain the same as in the full-scale plies; only their fiber count is changed. With the ply-thickness method a subscale laminate is produced using exactly the same number and sequence of plies and consequently the same number of interply bond lines, as used in the prototype (i.e., full-scale) laminate. The experimental part of this study is complemented with finite element analyses to predict the response and the buckling load of each panel. The failure modes are described for all of the panels tested.

Received 14 May 1999; revision received 4 April 2001; accepted for publication 22 April 2001.

*Senior Aerospace Engineer, Mechanics and Durability Branch, Structures and Materials Competency, Mail Stop 190. Senior Member AIAA.
†Senior Specialist Engineer, Structures Technology, M/S: 6H-CJ.

Test Specimens

The specimens were fabricated from commercially available Hercules, Inc., AS4 graphite fibers, preimpregnated with Hercules, Inc., 3502 epoxy resin (AS4/3502) and 7075 aluminum alloy ribs and shear ties. The full-, half-, and quarter-scale specimens were made from grades 190, 95, and 47.5 material, respectively. The different grades of material allowed scaling of the ply thickness while maintaining a constant resin volume fraction. Typical material properties for the AS4/3502 grade graphite-epoxy material system and 7075 aluminum are presented in Table 1. All of the specimens were fabricated with 18 plies in the skin, 18 plies in the web, and 18 plies in the cap of the longitudinal stiffeners. Stacking sequences for the skin, stiffener web, and stiffener cap are given in Table 2. The dimensions of all components of the full-scale panel were scaled by a factor of $\frac{1}{2}$ and $\frac{1}{4}$ for the half- and quarter-scale panels, respectively. The panel geometry is shown schematically in Fig. 1a. All of the specimens had five equally spaced longitudinal stiffeners secondarily bonded to the skin and four mechanically fastened ribs, equally spaced and located symmetrically about the horizontal centerline of the specimen. The L-section ribs were fabricated from 7075 aluminum alloy and were mechanically fastened to the cap of the longitudinal stiffeners. The ribs were also attached to the skin with aluminum shear ties that were located between the longitudinal stiffeners. For the sake of completeness and consistency, all fasteners that were used in fabricating the full-scale specimens were also scaled by a factor of $\frac{1}{2}$ and $\frac{1}{4}$ for the half- and quarter-scale specimens, respectively. The panel scale factor N, width w, length L, skin thickness t_s, longitudinal stiffener spacing b, and rib spacing L_f are summarized in Table 3 for all of the specimens. The cross-sectional geometry of the longitudinal stiffener is shown in Fig. 1b, the rib geometry is shown in Fig. 1c, and the shear-tie geometry is shown in Fig. 1d. The geometry of the longitudinal stiffeners and ribs for all of the specimens are summarized in Tables 4 and 5. The ends of each specimen were potted in an epoxy-based compound to prevent brooming of the graphite fibers during testing, and the potting

material was encased in an aluminum frame. The loaded ends of the specimens were machined flat and parallel prior to testing to ensure a uniform load application. A photograph of a typical panel is shown in Fig. 2. The unstiffened side of each specimen was painted white to reflect light so that a shadow moiré interferometry technique could be used to monitor out-of-plane deflections during testing.

Test Apparatus and Setup

Test specimens were loaded in compression using a hydraulic test machine. The specimens were flat-end tested without lateral edge supports because a longitudinal stiffener is located along each lateral edge. The out-of-plane deflections of each panel were constrained by discrete local attachments at the intersection of the longitudinal stiffeners with the two center ribs (i.e., a total of 10 point restraints). Electrical resistance strain gauges were used to monitor strains, and displacement transducers were used to monitor longitudinal in-plane and transverse out-of-plane displacements at selected locations. All electrical signals were recorded at regular time intervals during the tests. Also, each specimen's out-of-plane deflection pattern at different load levels was obtained using a shadow moiré interferometry technique.

Analysis

A finite element model was developed and used to perform both linear and geometrically nonlinear analyses of the response of the panels. The finite element model consisted of 8632 elements and 53,424 degrees of freedom. The model and the assumed boundary conditions are shown in Fig. 3 for a typical specimen. The material properties used in the analysis are listed in Table 1. The skin, stiffeners, ribs, and shear ties were all modeled with quadrilateral plate elements. The loading condition used in the analyses was a uniform compressive axial load at one end of the specimen. The out-of-plane deflections were constrained at the intersection of the

Table 1 Typical material properties

Property	AS4/3502	7075 aluminum
Longitudinal modulus, E_1, Msi	19.5	10.3
Transverse modulus, E_2, Msi	1.30	10.3
Inplane modulus, G_{12}, Msi	0.77	4.0
Major Poisson's ratio, υ_{12}	0.3	0.3

Table 2 Skin and stiffener laminates stacking sequences

Laminate	Stacking sequence
Skin	$[45, 90, -45, 0, \pm 45, 0, \pm 45]_s$
Stiffener web	$[45, 90, -45, 0_2, 45, 0, -45, 0]_s$
Cap	$[45, 90, -45, 0_2, 45, 0, -45, 0]_s$

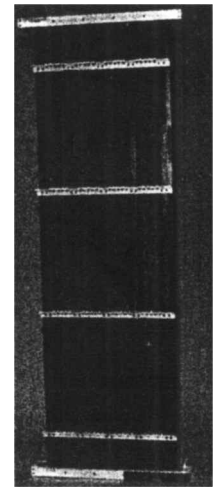

Fig. 2 Photograph of a typical test specimen.

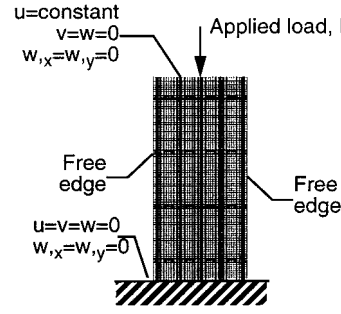

Fig. 3 Finite element model.

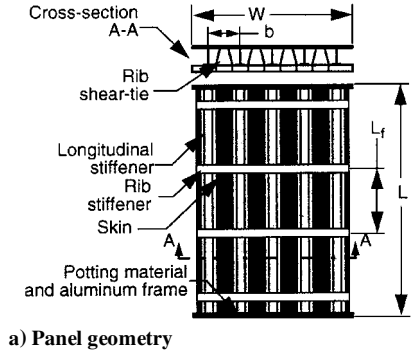

a) Panel geometry

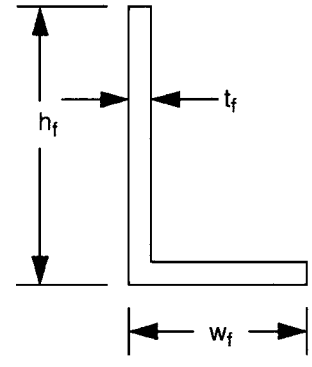

c) Rib stiffener

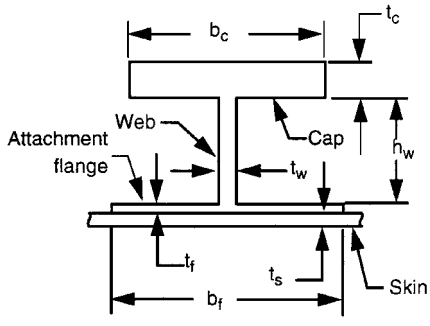

b) Longitudinal stiffener

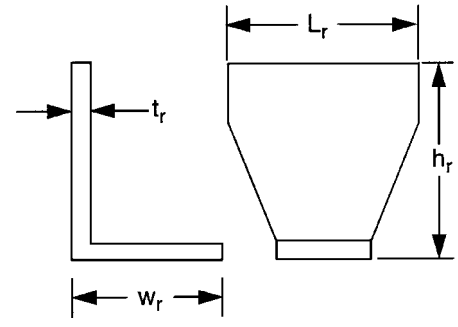

d) Shear tie

Fig. 1 Panel geometry and stiffener details.

Table 3 Test panel geometry

Specimen	Scale factor, N	Width W, in.	Total length L, in.	Skin thickness t_s, in.	Longitudinal stiffener spacing b, in.	Rib spacing L_f, in.
Quarter-scale	4	7.35	24.875	0.033	1.625	6.625
Half-scale	2	14.7	49.75	0.067	3.25	13.25
Full-scale	1	29.4	99.5	0.133	6.5	26.5

Table 4 Longitudinal stiffener geometry

Specimen	Cap width b_c, in.	Cap thickness, t_c, in.	Web height h_w, in.	Web thickness t_w, in.	Attachment flange width b_f, in.	Attachment flange thickness t_f, in.
Quarter-scale	0.343	0.033	0.375	0.033	0.783	0.017
Half-scale	0.685	0.067	0.750	0.067	1.567	0.034
Full-scale	1.370	0.133	1.500	0.133	3.133	0.067

Table 5 Rib and shear-tie geometries

	Rib geometry			Shear-tie geometry			
Specimen	Height h_f, in.	Width w_f, in.	Thickness t_f, in.	Height h_r, in.	Width w_r, in.	Thickness t_r, in.	Length l_r, in.
Quarter-scale	0.45	0.38	0.05	0.875	0.313	0.05	1.18
Half-scale	0.90	0.75	0.094	1.75	0.63	0.094	2.36
Full-scale	1.80	1.50	0.188	3.50	1.25	0.188	4.72

Table 6 Summary of results

		Analytical results		Experimental results			
Specimen	Scale factor, N	Buckling load P_{cr}, kips	End shortening at buckling u_{cr}, in.	Buckling load P_{cr}, kips	Buckling scaled load ratio	Failure load P_{ult}, kips	Failure scaled load ratio, $\alpha_{p,ult}$
Q1	4	12.01	0.80	12.00	1.038	14.25	1.020
Q2	4	12.01	0.80	12.00	1.038	14.75	1.056
Q3	4	12.01	0.80	12.00	1.038	15.64	1.120
H4	2	48.06	0.178	48.00	1.038	54.10	0.968
H5	2	48.06	0.178	48.00	1.038	57.10	1.022
H6	2	48.06	0.178	48.00	1.038	60.20	1.077
F7	1	192.16	0.336	185.00	1.000	223.50	1.000
F8	1	192.16	0.336	185.00	1.000	225.90	1.011

longitudinal stiffeners and the two inner ribs to simulate the lateral restraint system used in the tests. The linear buckling and geometrically nonlinear finite element analyses were performed using the structural analysis of general shells computer code.[6]

Results and Discussion

The test results for the quarter-, half-, and full-scale specimens are discussed subsequently. The experimental and analytical results are summarized in Table 6 for all of the specimens that were tested. The Q, H, and F prefixes on the specimen identification numbers identify quarter-, half-, and full-scale specimens, respectively. All of the specimens considered in this investigation were loaded to failure.

Experimental Results

The experimental load-shortening results are presented in Fig. 4. The measured end shortening u, normalized with respect to the specimen length L, is shown in the figure as a function of the normalized scaled load so that the response of all specimens can be directly compared. The scaled load ratio α_p is defined as

$$\alpha_P = N^2 \times P_N/P_1$$

where P is the applied load; N the geometric scale factor N = 1, 2, or 4 for the full-, half-, and quarter-scale specimen, respectively.

The solid circles in Fig. 4 represent the failure of each specimen. Failure is defined as the maximum load-carrying capability of the specimen. The experimental data suggest that all of the specimens buckled at approximately the same buckling strain. The scaled load ratios at failure $\alpha_{p,ult}$ listed in the last column of Table 6 indicate

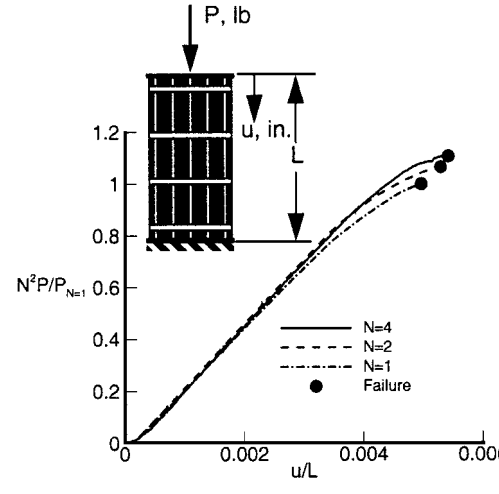

Fig. 4 Summary of normalized specimen end-shortening results from the experiments.

that the on the average the half- and quarter-scale panels supported approximately 4% more load then the full-scale panel prior to failure. This response is expected, as smaller scale panels often have fewer flaws or defects than their full-scale counterparts because of their smaller size.

The out-of-plane deflections w measured near the center of the specimens are shown in Fig. 5 as a function of applied load P for the quarter-, half-, and full-scale specimens. The deflection w is

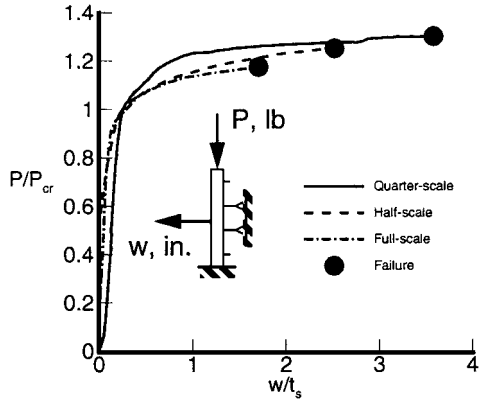

Fig. 5 Typical out-of-plane deflections at the center of the quarter-, half-, and full-scale specimens.

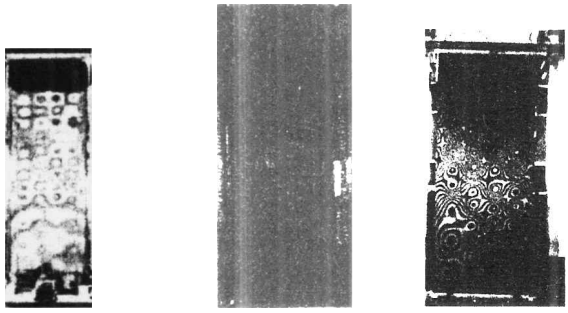

a) Quarter-scale specimen **b) Half-scale specimen** **c) Full-scale specimen**

Fig. 6 Moiré-fringe pattern of buckled skin just prior to failure.

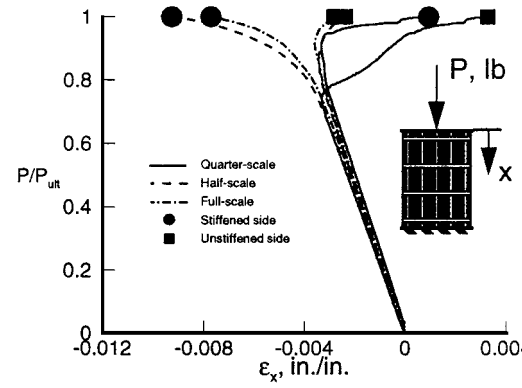

Fig. 7 Typical back-to-back surface strain results measured by strain gauges located on the skin and the cap of the central longitudinal stiffener.

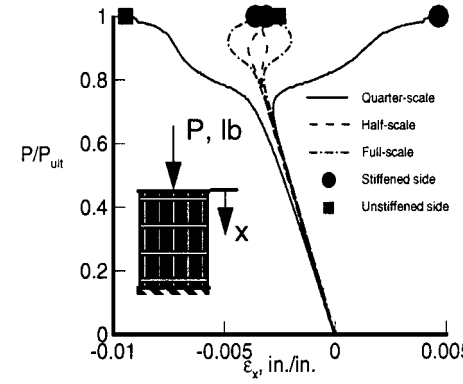

Fig. 8 Typical back-to-back surface strain results measured by strain gauges located on the skin midway between two longitudinal stiffeners.

normalized by the specimen's skin thickness t_s, and the applied load is normalized by the analytical buckling load P_{cr} calculated from a linear finite element analysis. A solid circle indicates failure of each specimen. The maximum normalized out-of-plane deflections are larger for the quarter- and half-scale specimens than for the full-scale specimens. The results indicate that the half- and quarter-scale specimens had more postbuckling capacity than the full-scale specimen. Specifically, the quarter- and half-scale panels were able to support as much as 30% and 20% more load, respectively, beyond buckling prior to failure than the full-scale specimen.

Typical moiré-fringe patterns for a quarter-, half-, and a full-scale panel just prior to failure are shown in Fig. 6. The moiré-fringe pattern for the quarter-scale specimen shown in Fig. 6a indicates that the panel buckled into five longitudinal half-waves in the center bay. In contrast, the moiré-fringe pattern for the half-scale panel, shown in Fig. 6b, indicates that in the center bay this panel buckled into only a single half-wave in both the longitudinal direction and across its width. The moiré-fringe results for the full-scale panel shown in Fig. 6c indicate that this panel has buckled into five half-waves along the length between the ribs and one half-wave between successive pairs of longitudinal stiffeners. The observed differences in the moiré-fringe patterns of the quarter-, half-, and the full-scale panel are most likely caused by inherent variations in the initial geometric imperfections of these panels. However, these differences did not seem to influence significantly the experimental buckling load of the panels.

A comparison of surface strain results as a function of applied load P, normalized by the applied load at failure taken from strain gauges located on the skin and the cap of the central longitudinal stiffener, is shown in Fig. 7. The solid, dashed, and dash-dot lines indicate surface strain results for the quarter-, half-, and full-scale specimens, respectively. The solid squares represent strain gauges located on the unstiffened side of the specimens, whereas the solid circles represent strain gauges on the stiffener cap. The results indicate divergence of the back-to-back gauges caused by bending of the specimens. The quarter-scale specimen results suggest that there was a redistribution of load soon after buckling occurred, as evidenced by the reduction in magnitude of the compressive strain on the skin side as this specimen was loaded to failure. The strain reduction on both sides of the panel may have been caused by separation of the skin from the stiffener (at the skin-stiffener interface) and subsequent outward buckling of both the skin and the stiffener.

A comparison of surface strain results as a function of applied load P, normalized by the applied load at failure taken from strain gauges located on the skin midway between two longitudinal stiffeners and midway between the two ribs, is shown in Fig. 8. The solid, dashed, and dash-dot lines indicate results for the quarter-, half-, and full-scale specimens, respectively. The solid circles and squares indicate failure of the specimens. The results indicate a significantly larger amount of bending in the quarter-scale specimen prior to failure. The higher bending strains for the quarter-scale panel are consistent with the fact that this specimen exhibited the highest postbuckling capability of the panels tested. For the half- and full-scale specimens the results in Fig. 8 suggest that a redistribution of load occurred in the skin between the longitudinal stiffeners prior to failure.

The longitudinal strain distribution across the horizontal centerline of the specimen at midlength for the quarter-, half-, and full-scale specimens are presented in Figs. 9a–9c, respectively, for two values of applied load P. In each figure the circles represent results from the stiffened side of the panel, and the squares represent those from the unstiffened side of the panel. The vertical dashed lines indicate the location of the centerline of the longitudinal stiffeners, where strain gauges on the stiffened side are actually located on the cap of the stiffeners. The strain results prior to buckling (i.e., at the lower P values) indicate a uniform strain distribution, as expected. After buckling, the surface strains are reduced in the skin and increased in the cap of the longitudinal stiffeners. The results for the half- and full-scale specimens were symmetric about the vertical centerline of the specimens; however, the result for the quarter-scale panel (Fig. 9a) indicates a nonsymmetric distribution

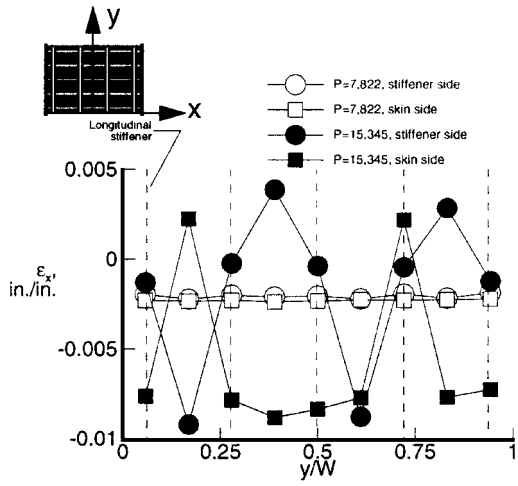

a) Quarter-scale panel

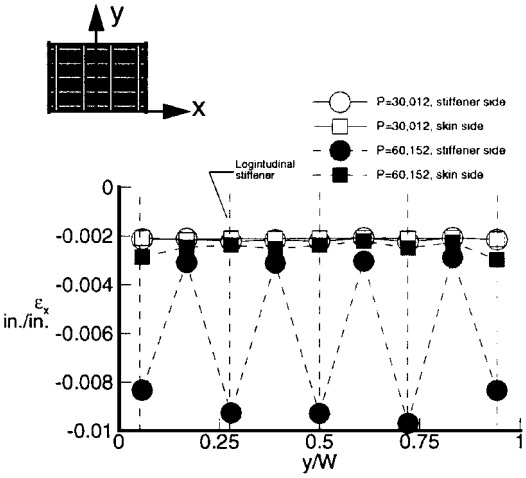

b) Half-scale panel

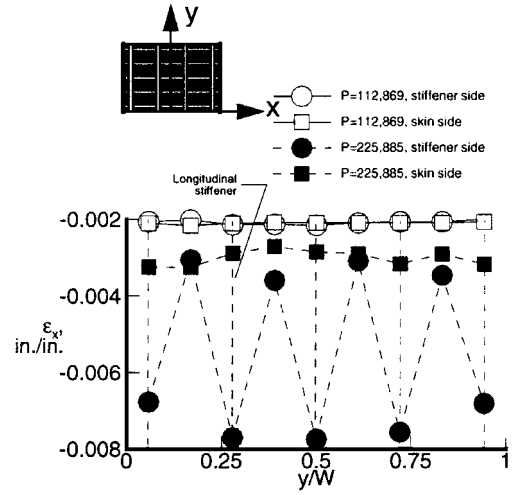

c) Full-scale panel

Fig. 9 Longitudinal surface strain distribution across panel midway between ribs for the skin and longitudinal stiffeners.

prior to failure. The nonsymmetry in the results for the quarter-scale panel was caused by the load redistribution that was discussed in connection with the plot of Fig. 7.

All of the specimens experienced the same type of failure. Post-failure photographs of the full-scale specimen F8 are shown in Figs. 10a and 10b. Failure of the panel was initiated in the cap of the stiffeners, which sustained the highest compressive stresses prior to failure (Fig. 10b). This initial failure event was immediately

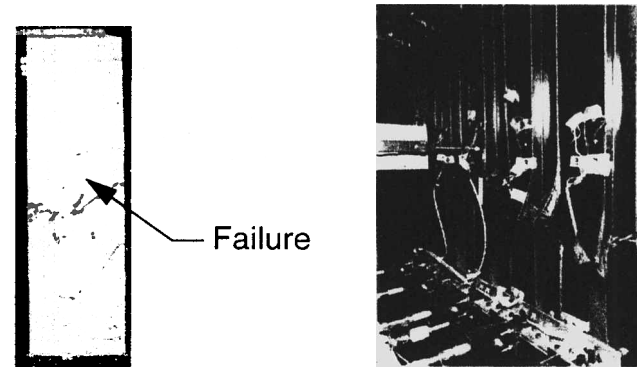

a) Skin-side view of panel b) Stringer-side view of panel

Fig. 10 Photograph of a failed full-scale panel.

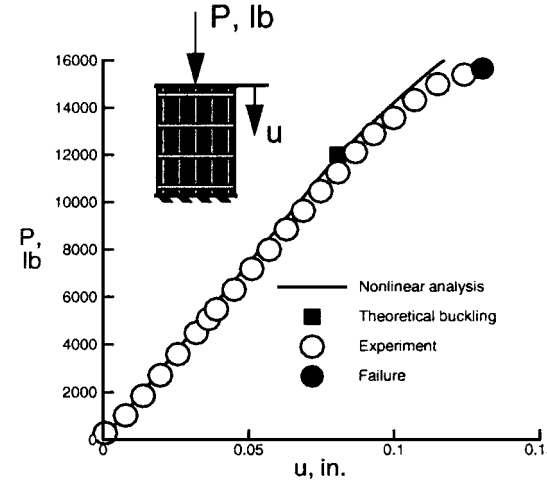

Fig. 11 Comparison of experimental and analytical end-shortening results for the quarter-scale panel.

followed by a redistribution of the internal load, which resulted in separation of the stiffeners from the skin in the damaged region and ultimately failure of the skin. As seen in Fig. 10a, the skin side failed as a result of a compression failure mode, with some brooming of the 45-deg plies in the skin. Also, significant cracking noises emanated from the specimen after buckling and prior to failure and may be attributed to the stiffener separating from the skin at the skin-stiffener interface.

The failure scaled load ratios $\alpha_{p,\mathrm{ult}}$, summarized in Table 6, indicate that the scale effects were fairly minimal and that strength scaling was achieved with very good accuracy. These results suggest that the ply-thickness approach to laminate scaling, which has been used in this investigation, is a reasonable approach to scaling composite structures loaded in compression. Many of the earlier studies (e.g., Refs. 1 and 5) that employed other laminate thickness scaling techniques noted significant strength scale effects, with scaled load ratios ranging from 1.07 to 1.83 (depending on the layup) in relation to quarter-scale models.

Analytical Results

Linear and geometrically nonlinear finite element analyses were performed for the specimens. A comparison of the analytical and experimental end shortening results u as a function of the applied load P for a quarter-scale specimen is presented in Fig. 11. The analytical buckling load is represented by a solid square. The solid line represents the end shortening results that were obtained from the analysis; the open circles represent the experimental results, and the failure load is indicated by a solid circle. The results in Fig. 11 indicate that the analysis accurately predicts the load-deformation response up to failure of the specimen.

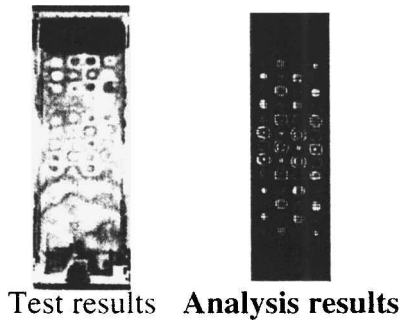

Fig. 12 Comparison of experimental and analytical out-of-plane deflection results for the quarter-scale panel.

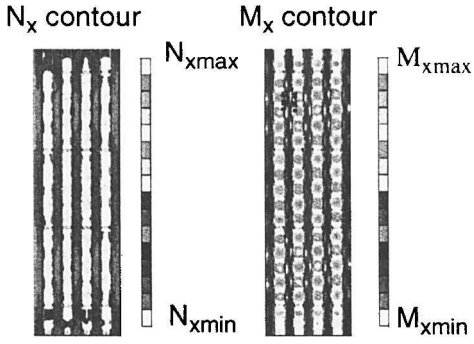

Fig. 13 Typical stress contours from nonlinear analysis of quarter-scale panel.

The out-of-plane deflection contours just prior to failure and a photograph of the corresponding moiré-fringe pattern for the skin side of the quarter-scale panel are presented in Fig. 12. The out-of-plane deflection contours compare well qualitatively with the moiré-fringe pattern. The analysis results accurately predicted the local skin-buckling mode of the specimen.

Typical stress resultant contours for the quarter-scale specimen, obtained from a geometrically nonlinear analysis just prior to failure, are presented in Fig. 13. The results indicate that in-plane stresses N_x are highest in regions where longitudinal stiffeners are bonded to the skin, and the bending stress resultants M_x about an axis perpendicular to the longitudinal axis are a maximum in the skin regions between longitudinal stiffeners.

Conclusions

An experimental and analytical investigation has been conducted to study the effects of geometric scaling on stiffened graphite-epoxy panels fabricated using the ply-thickness method of laminate scaling. Experimental results were presented for quarter-, half-, and full-scale specimens. A comparison of the end shortening results indicates a very good correlation between the gross stiffness response of subscale and full-scale specimens. The strength scale effects were also found to be minimal, with the ratio of the failure load of the scaled panel to the failure load of the full-scale panel times the square of the scale factor ranging from 1.02 to 1.12, with an average value of about 1.04. These results suggest that the accuracy and the reliability of the ply-thickness approach to laminate thickness scaling is reasonable. Failure was typically initiated in the cap of the stiffeners, which sustained the highest stresses prior to failure, and the initial failure was followed by local separation of skin-stiffener bond lines and ultimately ended with the failure of the skin in the panel center bay.

Analytical results obtained from nonlinear finite element analysis correlate well with experimental results up to failure. Analytical stress contours indicate that high in-plane longitudinal stresses occur at the stiffener-skin interface regions, as the specimens are loaded to failure. Also, high bending stresses occur in the skin of the buckled specimens, between the longitudinal stiffeners caused by redistribution of load resulting from postbuckling behavior and local damage. Because of this local damage, strain data from the experiments were not compared directly with the elastic analysis predictions. A progressive failure analysis is needed.

References

[1] Jackson, K. E., "Scaling Effects in the Static and Dynamics Response of Graphite-Epoxy Beam-Columns," NASA TM 102697, July 1990.

[2] Wisnom, M. R., "The Effect of Specimen Size on the Bending Strength of Unidirectional Carbon-Fibre-Epoxy," *Composite Structures*, Vol. 18, No. 1, 1991, pp. 47–63.

[3] Wieland, T. M., Morton, J., and Starnes, J. H., "Scale Effects in Buckling, Postbuckling and Crippling of Graphite-Epoxy Z-section Stiffeners," AIAA Paper 91-0912-CP, 1991.

[4] Deo, R. B., and Kan, H. P., "Effects of Scale in Predicting Global Structural Response," *Proceedings of First NASA Advance Composite Technology Conference*, Pt. 2, 1990, pp. 761–777.

[5] Kellas, S., and Morton, J., "Strength Scaling in Fiber Composites," NASA CR 4335, Nov. 1990.

[6] Rankin, C. C., Brogan, F. A., Loden, W. A., and Cabiness, H. D., "STAGS User Manual, Version 3.0," Lockheed Martin Missiles & Space Co., Inc., Rept. LMSC P032594, Palo Alto, CA, March 1999.